Methods xxx (2015) xxx–xxx

Contents lists available at ScienceDirect

Methods

journal homepage: www.elsevier.com/locate/ymeth

Preparation and characterization of aptamer–polyelectrolyte films and microcapsules for biosensing and delivery applications

Emily Mastronardi [1], Phepafatso K. Tsae [1], Xueru Zhang, Amanda Pach, Yasir Sultan, Maria C. DeRosa *

Department of Chemistry, Carleton University, 1125 Colonel By Drive, Ottawa, Ontario K1S 5B6, Canada

ARTICLE INFO

Article history:
Received 31 July 2015
Received in revised form 27 October 2015
Accepted 28 October 2015
Available online xxxx

Keywords:
Aptamer
Polyelectrolyte multilayers
Thin films
Microcapsules
Biosensing
Controlled delivery

ABSTRACT

"Smart" materials are polymer systems that are able to change their physical or chemical properties in response to external stimuli in their environment. By adding a specific molecular recognition probe to a polymer, hybrid materials can be developed that retain the properties of the advanced polymer and gain the ability to respond to a specific molecular target. Aptamers are single-stranded oligonucleotides that are well-suited to serve as molecular recognition probes due to the specificity and affinity of their target recognition as well as their stability and ease of synthesis and labeling. In particular, their negatively charged backbone makes for their facile incorporation into polyelectrolyte-based materials. This article will provide a brief review of the currently reported biosensor and delivery platforms that have been reported employing aptamer–polyelectrolyte materials, as well as a detailed description of the methods used to synthesize and study films and microcapsules containing small-molecule aptamer probes.

1. Introduction

Smart materials are a category of multifunctional materials capable of sensing a change in their environment and reporting it by changing their physical or chemical properties. Examples of these materials respond to many chemical and physical stimuli such as temperature, pH, and electric fields, making them useful in sensing applications [1]. Incorporation of a molecular recognition probe, such as antibodies or aptamers, into these materials could impart the recognition ability from the probe to the material as a whole, creating bioresponsive materials [2]. Aptamers, single-stranded oligonucleotides that can bind targets specifically and selectively, are ideal candidates for incorporation into smart materials. They are synthesized chemically at a relatively low cost, and can be chemically modified at precise locations with a variety of functional groups and reporter molecules, making them highly compatible with polymeric materials and easily adapted to smart material applications. Furthermore, as aptamers are nucleic acids, their structure and binding can also be regulated by the addition of a complementary DNA strand, adding another layer of control to the smart material response. To exploit these characteristics, aptamers have been integrated into a variety of polymeric, dendrimeric, and nanoscale systems, yielding target-responsive materials [3–7].

Polyelectrolyte multilayer (PEM) films and microcapsules belong to a family of multifunctional materials from which many smart materials have been developed. The layer-by-layer (LBL) method for film deposition described by Decher provides a simple technique with which to create PEM films [8]. Nanoscale thin films are created by the alternating adsorption of negatively and positively charged polyelectrolytes onto a charged surface. DNA's negatively charged backbone allows for its simple incorporation into polyelectrolyte films through electrostatic interactions. DNA has been readily incorporated into polyelectrolyte films and capsules for applications such as Hepatitis B DNA detection [9] and gene delivery [10–13]. Thus, the incorporation of DNA aptamers into polyelectrolyte films is a feasible approach to the generation of bio-responsive films for sensor and controlled delivery applications.

The first demonstration that an aptamer incorporated into a PEM film could retain its ability to bind its target came in 2009, where the aptamer's recognition of a dye target was conferred to the whole film with only a minor reduction in binding affinity [14]. Since this initial report, other aptamer-PEM biosensors and smart materials have been reported. The PEM can serve as a simple platform for an aptamer sequence, as was described in a report on an electrochemical aptasensor for the D enantiomer of arginine vasopressin (D-VP) [15]. In this case, aptamer-target binding does not effect a structural or chemical change within the polymer matrix. Alternatively, when the aptamer is embedded within the polyelectrolyte matrix, biosensors can be developed that exploit

* Corresponding author.
E-mail address: maria.derosa@carleton.ca (M.C. DeRosa).
[1] These authors contributed equally to this work.

http://dx.doi.org/10.1016/j.ymeth.2015.10.018
1046-2023/

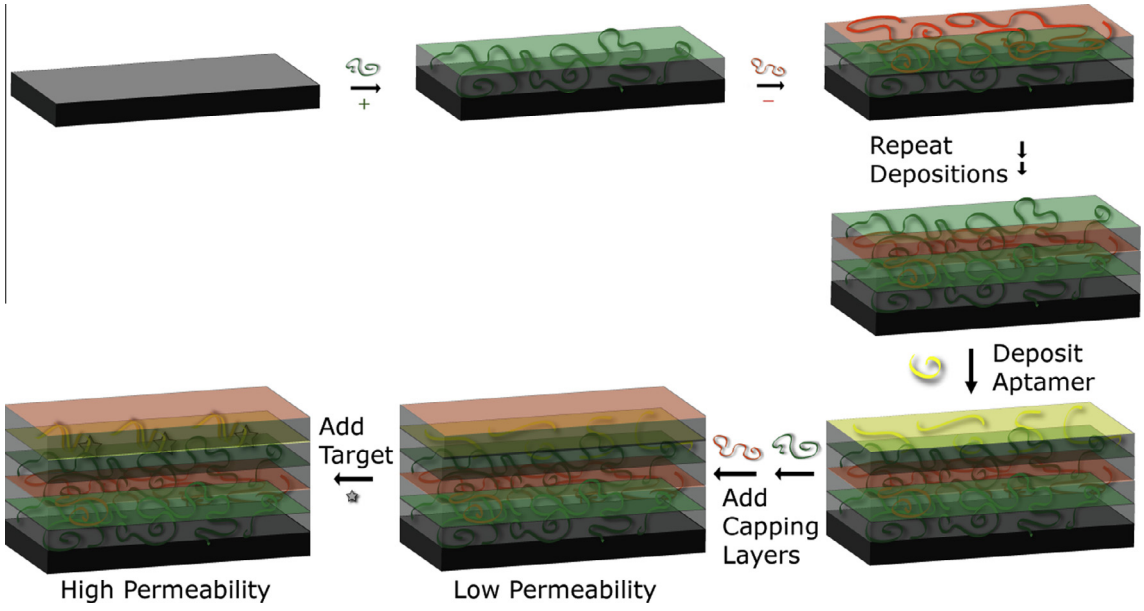

Fig. 1. Preparation of an aptamer-embedded PEM film system. A charged surface (e.g. glass or quartz slide, modified gold electrode, etc.) is sequentially exposed to oppositely charged polyelectrolytes (green and orange ribbons), with alternating rinses, to prepare a base layer. At a desired number of base bilayers, an aptamer sequence (yellow ribbons) is substituted for the negatively charged polyelectrolyte and a fixed number of aptamer-containing bilayers are deposited. The film is capped with a standard polyelectrolyte bilayer. In the absence of the aptamer's cognate target (gray star), the film has limited permeability. Target binding and concomitant structural changes to the aptamer and the PEM lead to an increase in permeability.

the smart material's response. Aptamer-embedded PEM thin films have been used as gatekeepers in a plasmonic nanoparticle visual sensor [16]. A similar mechanism was recently exploited to create an electro-chemiluminescence sensing platform for bisphenol A (BPA) using aptamer-induced permeability change within a polyelectrolyte smart material [17]. While the previously reported PEMs were built from synthetic polyelectrolytes, the generality of aptamer-PEM systems has recently been demonstrated by the successful incorporation of an aptamer into a PEM system comprised of natural polyelectrolytes [18]. Microcapsules based on smart aptamer-PEM systems have also been investigated; the aptamer-target binding event was shown to alter the diffusive properties of the film, with target-binding increasing the flux through the microcapsules [19]. More recently, aptamers have also been employed as collapsible scaffolds for PEMs that undergo target-induced rupture [20].

The ease and utility of aptamer incorporation into PEM systems warrants the investigation of aptamer-PEM smart materials for a variety of applications in medicine, environment, and agriculture [21]. The objective of this paper is to provide the methodology for creating and characterizing aptamer-PEM films and microcapsules for sensing and delivery applications. Three smart material systems will be described: (1) aptamer-embedded polyelectrolyte films (Fig. 1), where the aptamer substitutes for a negatively charged polyelectrolyte within a PEM system (2) aptamer-embedded polyelectrolyte microcapsules (Fig. 2), where the walls of a hollow microcapsule contain aptamers as a recognition agent, and (3) aptamer-loaded polyelectrolyte microcapsules (Fig. 3) where the aptamers are scaffolds within the hollow core of the microcapsule. The aptamers that will be described herein are for small molecule targets such as SB dye for easy visualization.

2. Material and methods

2.1. List of materials

The sulforhodamine B aptamer (SA sequence: 5′-CCG GCC TAG GGT GGG AGG GAG GGG GCC GG-3′), the lysine aptamer (LA sequence: 5′- ATA CCA GCT TAT TCA ATT TGA GGC GGG TGG GTG GGT TGA ATA CGC TGA TTA CCC CAT CGG AGA ACG TTA AGG CGC TTC AGA TAG TAA GTG CAA TCT-3′) and a random oligomer (RO) (RO sequence: 5′-GAC CTA TGA TAG CAT CAG TCG CAT CAG TC-3′) were synthesized on a MerMade 6 oligonucleotide synthesizer using standard phosphoramidite chemistry [22] and DNA synthesis reagents from Glen Research and Controlled Pore Glass (CPG) columns from BioAutomation were used as received. These three sequences were also synthesized with fluorescein phosphoramidite (6-FAM, Glen Research) added to the 5′ ends. Oligonucleotides were purified by polyacrylamide gel electrophoresis (12%) and mass confirmed by ESI-MS (Novatia). Calf thymus DNA (CT, sodium salt, type I) was purchased from Sigma–Aldrich and also used in control films.

Target molecules sulforhodamine B dye (SB) and L-lysine were purchased from Sigma–Aldrich, as well as non-specific control target, L-histidine. Non-specific control molecule tetramethylrosamine (TMR) was purchased from Invitrogen. Polyelectrolytes of varying composition and molecular mass were used for these experiments. Poly(diallyldimethylammonium chloride) (PDDA, MW $\leqslant$ 100,000 Da), poly(sodium 4-styrene-sulfonate) (PSS, MW 100,000 and 70,000 Da), poly(allylamine hydrochloride) (PAH, MW $\approx$ 56,000 Da) were all purchased from Sigma–Aldrich and used without further purification. Hyaluronan (HA, MW 1,580,000 Da), purchased as sodium hyaluronate, and chitosan (CHI, MW 135,000 Da) were purchased from Acros Organics. Sodium carbonate (Na_2CO_3; >99.5%), ethylenediaminetetraacetic acid (EDTA; 99%), anhydrous calcium chloride ($CaCl_2$, $\geqslant$93.0%), and sodium bicarbonate ($NaHCO_3$, $\geqslant$99.5%) used for fabrication of $CaCO_3$ templates, were all purchased from Sigma–Aldrich (Oakville, ON). Potassium ferricyanide ($K_3Fe(CN)_6$; 99%) and hexaammineruthenium chloride ($Ru(NH_3)_6Cl_3$; 98%) for electrochemistry experiments were obtained from Sigma–Aldrich. 2-Mercaptoethylamine hydrochloride (>98%) for electrode modification was obtained from Alfa Aesar.

Deionized water was used for all buffer preparations and buffers filtered through Corning 0.22 μM cellulose acetate filter units before use. All glassware was rinsed in distilled water 5 times, fol-

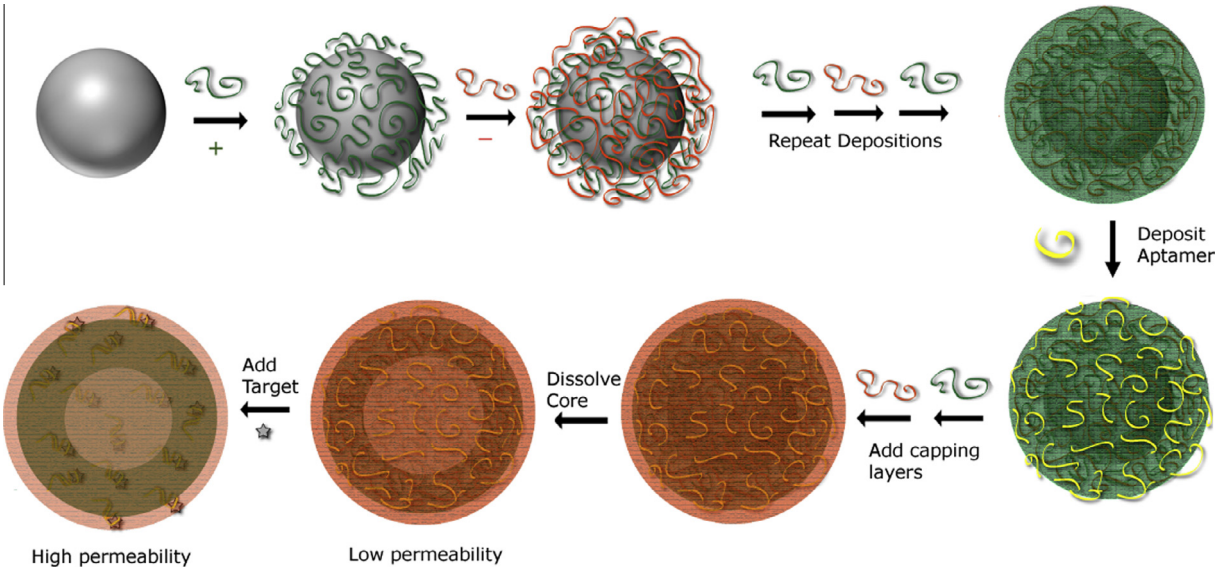

Fig. 2. Preparation of an aptamer-embedded PEM microcapsule. A sacrificial spherical template ($CaCO_3$) is sequentially exposed to oppositely charged polyelectrolytes (green and orange ribbons), with alternating rinse steps, to prepare a base layer. At a desired number of base bilayers, an aptamer sequence (yellow ribbons) is substituted for the negatively charged polyelectrolyte and a fixed number of aptamer-containing bilayers are deposited. A standard polyelectrolyte bilayer is used to cap the aptamer layers. The core is then dissolved, yielding a hollow microcapsule containing embedded aptamers within its wall. In the absence of the aptamer's cognate target, the microcapsule wall has limited permeability. Once again, target binding and concomitant structural changes to the aptamer and the PEM lead to an increase in permeability through the microcapsule wall.

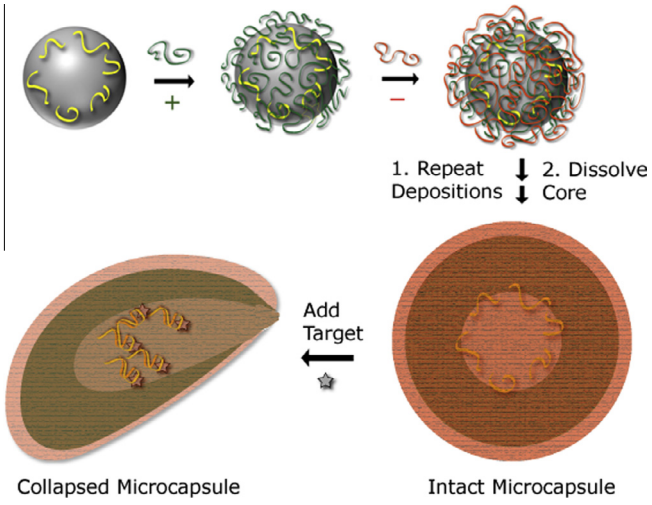

Fig. 3. Preparation of an aptamer-loaded PEM microcapsule. Aptamer-doped (yellow ribbons) $CaCO_3$ microparticles are used as the sacrificial spherical template for microcapsule preparation. The microparticles are sequentially exposed to oppositely charged polyelectrolytes (green and orange ribbons), with alternating rinse steps, to prepare a base layer. At a desired number of bilayers, the core is dissolved and the aptamer sequence serves as a scaffold to support the PEM microcapsule wall. In the absence of the aptamer's cognate target, the microcapsule is stable. Target binding and concomitant structural changes to the aptamer lead to a collapse of the microcapsule.

lowed by 5 rinses in deionized water before use. Glass (76 mm × 25 mm) and quartz slides (75 × 25 mm) were purchased from VWR. The slides were cut (~1.5 mm × 2.5 mm) using a hand-held diamond-tipped glass cutter.

2.2. Aptamer-embedded PEM film preparation methods

2.2.1. Dip-coating on slides

The layer-by-layer technique described by Decher [8] was utilized to create PEM films. The specific deposition conditions may need to be optimized depending on the aptamer system selected. The conditions used to generate SA films are described. Glass and quartz slides were cleaned using a 1:1:5 solution of H_2O_2:NH_4OH:H_2O at 70–90 °C for 10 min, and washed with water before deposition. PEM films composed of synthetic polyelectrolytes were prepared as follows. Slides were washed with water and dipped into solutions of oppositely charged polyelectrolytes for 20 min each, beginning with PDDA (5 mg/mL in 0.2 M NaCl) followed by PSS (5 mg/mL in 0.2 M NaCl). The slides were washed with water in between each polyelectrolyte deposition step. This was repeated for five cycles, resulting in five bilayers of PDDA and PSS (samples of these films where nothing further was deposited were also used as controls). Films containing DNA repeated this cycle five more times, using DNA as the anionic layer in place of PSS. All DNA samples were heated to 90 °C in deposition buffer (20 mM Tris–HCl, 0.2 M NaCl, pH 7.4) for 5 min and left to cool to room temperature prior to deposition. The slides were placed in a solution of DNA (6 μM for SA; 11 μM for RO; 0.04 μM for CT) in deposition buffer for 20 min at room temperature. To protect the DNA, an additional capping bilayer of PDDA/PSS was deposited, and the slides were dried for at least 5 h at room temperature prior to additional experiments. Films of the following composition were made $(PDDA/PSS)_5(PDDA/SA)_5(PDDA/PSS)$, $(PDDA/PSS)_5(PDDA/RO)_5(PDDA/PSS)$, and $(PDDA/PSS)_5(PDDA/CT)_5(PDDA/PSS)$. Films were annealed by heating in 0.1 M KCl at pH 7.4 at 70 °C for 10 min and leaving to cool to room temperature.

PEM films composed of natural polyelectrolytes required some modification to the original deposition procedure. Chitosan (CHI) and hyaluronan (HA) solutions were prepared at 1 mg/mL in 0.15 M NaCl, and the pH adjusted to 4.5 using diluted glacial acetic acid to ensure both polyelectrolytes were charged. The slides were dipped successively into 10 mL solutions of CHI and HA for 15 min, while rinsing twice with 0.15 M NaCl pH 4.5 (first rinse 10 s, second rinse 5 s) in between polyelectrolytes. Rinsing time proved to be critical to the linear growth of the films, as well as the target binding (see Section 3.2). Films made using DNA as the negative polyelectrolyte used a 2 μM solution of SA or RO in 0.15 M NaCl pH 4.5 and the solutions were heated to 80–90 °C for 15 min, fol-

lowed by cooling on ice for 30 min to allow proper aptamer folding. Using this deposition method, films with the following compositions were made: $(CHI/HA)_{10}(CHI/SA)_5(CHI/HA)$ for the aptamer-containing films, and $(CHI/HA)_{10}(CHI/RO)_5(CHI/HA)$ for the films containing random oligonucleotides. Annealing was found to be detrimental to the films (see Section 3.3) thus it was avoided.

2.2.2. Dip coating on electrodes

Gold electrodes (1.6 mm) were rinsed with water and polished with 1 μm diamond slurry polish, followed by rinsing with water. The working electrode was then etched three times in 1 M H_2SO_4 in a Ag/AgCl|Pt 3-electrode system cycling from −0.25 to 1.65 V using a CH Instruments 660C Electrochemical Analyzer. Multiple polishing steps (3–4) as well as fresh H_2SO_4 every time greatly improved film deposition. The surface of the gold electrode was functionalized with a positively charged species using 100 μL of 5 mM 2-mercaptoethylamine hydrochloride (>98%) in anhydrous ethanol. The electrode was incubated in this solution for 50 min, replacing with fresh solution every 5 min. The electrode was rinsed with 10 mL of ethanol. The layer-by-layer method was then used to deposit alternating polyelectrolytes (PAH or PSS; 2 mg/mL in NaCl, pH 7.4) and oligonucleotides (1 μmol SA or RO in 0.5 M NaCl, pH 7.4) onto the gold electrode. The DNA was pre-heated to 70 °C and allowed to cool to room temperature prior to deposition. The films deposited onto the electrode included: $(PAH/PSS)_4$ and $(PAH/SA)_2(PAH/PSS)_2$ as a controls, and $(PAH/SA)_2(PAH/PSS)_2$ as our aptamer-PEM system.

2.3. Aptamer-embedded and aptamer-loaded PEM microcapsule preparation methods

2.3.1. Preparation of sacrificial templates for microcapsule deposition

Synthesis of PSS-doped calcium carbonate (PSS-$CaCO_3$) spheres for the preparation of aptamer-embedded microcapsules was done following an established protocol [23]. Briefly, 200 mg of PSS was added to 50 mL of 0.33 M calcium chloride ($CaCl_2$) in deionized water and this was mixed with an equal volume of 0.33 M Na_2CO_3 in deionized water in a 2 L beaker, with 1 min of rapid stirring (1100 rpm, using a magnetic stir bar). The solution was allowed to sit undisturbed for 10 min with the precipitate collecting at the bottom of the beaker. The PSS-$CaCO_3$ precipitate spheres were then filtered under vacuum, washed with deionized water and air dried overnight.

The synthesis of aptamer-doped templates for the preparation of aptamer-loaded PEM microcapsules required modifications to the original procedure. Efficient preparation of aptamer-loaded templates required preparation in smaller batches and with modified conditions over the PSS-doped cores. PSS (0.13 mg) and SA (0.64 mg) were first dissolved in 500 μL of 0.33 M $NaHCO_3$ solution in deionized water. This was mixed with 500 μL of 0.33 M $CaCl_2$ solution in deionized water under vigorous stirring (1000 rpm) at 10 °C for 20 s. The solution was then left undisturbed for 6 min. The SA:PSS-$CaCO_3$ particles were then filtered under vacuum, washed with deionized water and dried overnight.

2.3.2. PEM deposition on $CaCO_3$ templates

Aptamer-embedded PEM microcapsules were prepared as follows. PSS-$CaCO_3$ spheres (10 mg) were dispersed in 1 mL of 2 mg/mL cationic polyallylamine hydrochloride (MW 56,000 Da) in 0.5 M NaCl. Spheres were then shaken gently for 10 min, followed by centrifugation at 1.6*g* for 2 min. Following removal of supernatant, the spheres were suspended in 1 mL of water and centrifuged using the same conditions as above for a total of five washings per layer added. For the anionic polymer layer, either 1 mL of 2 mg/mL PSS (MW 100,000 Da) in 0.5 M NaCl or oligonucleotides (SA or RO; 0.3 μM in 10 mM Tris–HCl, pH 7.3) were deposited in alternating layers with PAH following same protocol described above. $(PAH/PSS)_3(PAH/SA)_1(PAH/PSS)_1$, $(PAH/PSS)_5$ and $(PAH/PSS)_3(PAH/RO)_1(PAH/PSS)_1$, microcapsules were prepared by this method. The sacrificial cores were dissolved by dispersing the coated templates in 1 mL of 500 mM EDTA in 500 mM Tris buffer, pH 7.3, with gentle stirring overnight. This step was repeated three times to ensure complete removal $CaCO_3$ cores. Isolation of microcapsules was done by centrifugation at 0.6*g* for 1 min and washing with a total volume of 5 mL of water to ensure total removal of any remaining EDTA. Storage of microcapsules as a suspension in Tris buffer pH 7.3 was found to keep them stable for at least two weeks. Samples were annealed at 70 °C for 10 min and cooled to room temperature prior to any binding experiments. Aptamer-embedded PEM microcapsules containing LA required some modifications to the above procedure in order to be prepared. Specifically, $(PAH/PSS)_3(PAH/LA)_1(PAH/PSS)_1$ microcapsules were prepared by depositing all components in a 0.8 M NaCl solution, instead of 0.5 M NaCl.

Aptamer-loaded PEM microcapsules were prepared as follows. 1 mg of SA: PSS-$CaCO_3$ particles were incubated alternatively in 1 mL of PDDA (3 mg/mL in 0.5 M NaCl) and either 1 mL of PSS (3 mg/mL in 0.5 M NaCl) for 30 min each to constitute (PDDA/PSS) films. Washing with deionized water after each layer deposited was achieved by incubating the particles in 1 mL of deionized water for 1 min, followed by centrifugation as described above, repeated three times. After five PDDA/PSS bilayers were deposited, microcapsules were obtained by dissolving the sacrificial SA:PSS-$CaCO_3$ templates by overnight incubation in 0.5 M EDTA, pH 6.97. This high concentration of EDTA was crucial to completely remove all of the $CaCO_3$. Excess EDTA was removed by washing extensively with deionized water.

2.4. Characterization of aptamer-embedded PEM films

2.4.1. Monitoring polyelectrolyte deposition

UV–Vis analysis (Cary 300 Spectrophotometer with a home-modified cuvette holder for slides) was used to monitor bilayer deposition on glass or quartz slides. The growth of CHI/HA bilayers was examined by monitoring the absorbance of glucosamine and N-acetylglucosamine at 190–220 nm, while PDDA/PSS bilayers could be tracked by monitoring the styrene moiety absorbance at 220 nm. DNA deposition can be monitored by following the absorbance at 260 nm. Before the films were analyzed after layer deposition, an additional rinse in water (10 mL, 1 min) was performed to remove excess salt, and the films were dried under argon.

Electrochemical techniques (CH Instruments 660C Electrochemical Analyzer) were also used to track the growth of bilayers on gold electrodes by observing the decrease in ferricyanide peak current as the number of deposited bilayers increased. A 3 electrode system for cyclic voltammetry was used (gold working electrode, platinum wire counter electrode, Ag/AgCl reference) with KCl (0.5 M) as the electrolyte and $K_3Fe(CN)_6$ (0.5 mM) as the redox active probe. All solutions were purged with argon for 5 min before measurements began. Three cycles from 0.6 to −0.3 V (vs. Ag/AgCl) were run at 100 mV/s after each bilayer deposition.

Quartz crystal microbalance (QCM) can also be employed to confirm depositions, in this case on a quartz crystal. A quartz crystal microbalance (QCM) from Stanford Research Systems (QCM200, 5 MHz AT-cut quartz crystal oscillator with 0.1 s gate time) was used. Using the same deposition procedure described for quartz slides, films were deposited onto the quartz crystal. The change in relative frequency was used to monitor film growth, nulling capacitance by manually controlling the bias voltage required by the varactor.

After deposition, microscopy techniques were employed to determine film thickness and morpohology. Scanning Electron

Microscopy (SEM) images were taken at room temperature using a Tescan VegaII XMU SEM. The images were taken on dry films that were sputter-coated with a gold/palladium alloy using an Anatech Hummer VII Sputter-Coater (Richmond, Canada) prior to imaging. AFM images were taken from at least two areas of dry films (n = 3 or more) at room temperature, with a Ntegra AFM (NTMDT, Moscow, Russia) in tapping mode using 100 × 100 μm^2 scanner (Ntegra) and rotated monolithic Si cantilever tips (Budget Sensors; 125 μm long, 40 N'm spring constant Tap 300A1, 315 kHz resonance frequency).

2.4.2. Monitoring target binding, affinity, and specificity

SB binding of the synthetic PEM films and specificity against a non-target molecule, TMR, was monitored by UV–Vis spectroscopy (Cary 300). Aptamer-embedded and control films were dipped in 2 mM SB or TMR (in either water or 0.1 M KCl) and the absorbance of the films at 570 nm was monitored. The ratio of the 570 nm absorbance to the 260 nm absorbance of DNA was used for all comparisons to account for any differences in DNA loading between the films.

Both the synthetic and natural PEM films were also characterized using Confocal Laser Scanning Microscopy (CLSM) or Fluorescence Microscopy (FM) to determine target binding and specificity. CLSM (performed in air) was used to examine the distribution of SB within the PDDA/PSS family of PEM films. Annealed films were incubated in 2 mM SB or TMR in 0.1 M KCl for 30 min, followed by washing with deionized water until the washings were clear. A Zeiss LSM510 microscope was used (532 nm, 3% laser intensity for PDDA/PSS/SA and PDDA/PSS/RO films, 5% laser intensity for PDDA/PSS/CT film) with a Plan-Apochromat 63×/1.4 Oil Dic objective and LP950 filter, λ_{ex} 556 nm, while images were collected at λ_{em} 575 nm. The images were examined and brightness assessed using Adobe Photoshop CS2 (V. 9.0.2). The mean intensity values (obtained with histogram tool) were compared. The CHI/HA/DNA family of films were submerged in 200 μM SB dye (in 0.10 M KCl) for 30 min and rinsed for 10 s with 10 mL of deionized water 3 times. An EVOS FL fluorescent microscope was used for target-DNA colocalization experiments, using the green channel (λ_{ex} 470 nm, λ_{em} 525 nm) and the red channel (λ_{ex} 531 nm, λ_{em} 593 nm) for imaging the fluorescence of 6-FAM DNA and SB dye, respectively. Dye binding was imaged with 10× magnification using an Olympus BX61 Fluorescent microscope (λ_{ex} 531 nm, λ_{em} 594 nm) with a Q-imaging Retiga 2000R camera. The mean fluorescent intensities from each image were calculated using ImageJ, and Excel was used to conduct student t-tests (heteroscedastic analysis with unequal variance and 95% confidence interval).

Time-of-Flight Secondary Ion Mass Spectrometry (ToF-SIMS) was used to collect depth profiles of all PEM films to confirm composition and target binding. Depth profiles of dry films (both synthetic and natural) were obtained using a ToF-SIMS IV instrument (IonTOF GmnH, University of Alberta), collecting both positive and negative ion profiles from multiple locations on the surface. A dual ion-beam system was used to generate negative secondary ions, with Bi^+ ions (operated at 25 kV) used as an analytical source and Cs^+ ions (operated at 250 V for natural PEM films and 500 V for synthetic PEM films) used as a sputtering source. Craters were created in the films using alternating ion beams, and the center of the crater was used for ion acquisition. To generate surface images, the ToF-SIMS was operated at 25 kV in static mode, using Bi^+ ions as the analytical source, and optical images were taken using a digital camera attachment. Charge compensation by electron flooding was also employed during profiling since the samples were nonconductive.

QCM was also used to determine target binding to PEM films. For K_d experiments, 1 mL solutions of SB (from 0.001 to 10 mM, 0.1 M KCl) were added to the quartz crystal (following film deposition) for 30 min. The crystal was washed with water, dried with argon for 3 min, and the change in frequency was observed. The solver feature of Microsoft Excel was used to determine K_d values, by minimizing the residual values between the calculated and observed Δ frequency data.

2.4.3. Monitoring effects of target binding on PEM film permeability

Electrochemistry (CH Instruments Electrochemical Analyzer) was used to determine the effect of target binding on the diffusion of a redox active probe through the synthetic PEM films. Once again, a 3 electrode system for cyclic voltammetry was implemented, using KCl (0.5 M) as the electrolyte, $Ru(NH_3)_6Cl_3$ (0.5 mM) as the positively charged probe redox active probe, sulforhodamine B dye (100 μM) as the target, and tetramethylrosamine (100 μM) as the negative control. All solutions were purged with argon for 5 min before measurements began. The peak current (I_p) was extracted using semi-derivative analysis yielding better sensitivity. The surface area was calculated prior to film deposition using the CV trace from a 1 M H_2SO_4 etch with a 200 mV/s sweep rate (Surface Area = peak current (C)/charge (C/cm^2) where charge = 50 μC/cm^2 at 200 mV/s). The peak current (I_p) of the redox probe in the different films was extracted from CV curves (−0.15 to −0.35 V for $Ru(NH_3)_6Cl_3$). Diffusion coefficients were calculated using the formula: $I_p = 2.69\times 10^5 n^{3/2} A D^{1/2} [O] v^{12}$, where I_p = current (A), A = area of the electrode (cm^2), D = diffusion (cm^2/s), $[O]$ = the concentration of electroactive probe (mol/cm^3) and v = scan rate (V/s). For these experiments, n = 1 (attributed to the loss or gain of one electron per electroactive molecule). Microsoft Excel 2007 was used to conduct a standard t-test using the average of 3 calculated diffusions, 2 tails and two-sample equal variance (homoscedastic).

2.5. Characterization of aptamer-embedded and aptamer-loaded PEM microcapsules

2.5.1. Characterization of morphology and composition of sacrificial templates and PEM microcapsules

SEM with Energy Dispersive X-ray Spectroscopy (EDX) were used to characterize the templates as well as the resultant microcapsules after PEM deposition, before and after template dissolution. A Tescan VegaII XMU SEM with Secondary Electron Detector was used. The dried samples were uniformly spread on aluminum stubs and sputtered with a thin layer of gold film before measurements. The elemental analysis was conducted on an Oxford EDX instrument with INCAx-act Detector. INCA Energy software was used for analysis. The Tescan VegaII XMU Cryo stage SEM with Back Scattered Electron (BSE) Detector in Low Vacuum Environment under 10 Pascal nitrogen pressure at −30 °C was used to examine hydrated microcapsule samples. The hydrated samples were pre-frozen at −80 °C to preserve their morphologies. The percentage of ruptured, collapsed or swollen microcapsules in each sample was calculated by dividing the number of ruptured, collapsed or swollen microcapsules by the total number of microcapsules in that sample. At least three images of each sample obtained from different areas were counted; normally in each image more than 100 microcapsules were examined.

Confocal microscopy (Zeiss LSM510) was also used to characterize the templates and microcapsules containing 6-FAM-labeled SA or RO. Sample preparation for confocal microscopy studies involved placing 10 μL of solution on a clean microscope slide. A coverslip was placed on top with nail polish at the corners so that upon polish drying, the coverslip would be elevated from the microscope slide, keeping microcapsules from being crushed and thus allowing for wet sample imaging. FAM was excited at

489 nm, 20% intensity and/or SB was excited at 561 nm, 0.5–20% laser intensity.

Zeta potential measurements were also employed during microcapsule preparation to determine the best conditions (ionic strength, pH, polyelectrolyte concentrations) for depositions and to monitor their progress. Zeta potential measurements were done on Malvern Zetasizer 3000HS instrument at 25 °C in distilled water.

2.5.2. Monitoring target binding in PEM microcapsules

Tests with the SB dye were performed by incubating 1 μL of the aptamer-embedded PEM microcapsules at 1.09 x10^7microcapsules/mL for 30 min in 50 μL of a 10 μM solution (0.1 M KCl) of either SB or TMR followed by deposition (10 μL) onto a microscope slide. After drying overnight, samples were mounted in Fluoromount G from EMS (Hatfield, PA) and covered with a high performance coverslip of 0.17 mm thickness from Zeiss (Toronto, ON). Fluorescence was observed using the laser Argon/2 excitation line 488 nm with emission BP (Band Pass) 505–550 nm for fluorescein and exciting laser DPSS 561 with emission LP (Long Pass) 575 nm for SB and TMR. Z-stack images of samples were obtained by taking many slice images at approximately 0.8 μm intervals along the *Z*-axis.

2.5.3. Monitoring effects of target binding on microcapsule wall permeability or integrity

Permeability changes in the wall of the aptamer-embedded PEM microcapsule were monitored by Fluorescence Recovery After Photobleaching (FRAP). Unlabeled aptamer samples were used to prevent any overlapping emission of FAM with SB emission during FRAP. On average, eight microcapsules were monitored per sample ($n = 3$), using 10 μM SB in 0.1 M KCl. Sample bleaching was achieved by using various laser intensities with the 561 nm laser depending on the amount of dye inside the microcapsules. Recovery collection was performed at 1 s intervals with 0.5–12% laser intensity. Microcapsules with total fluorescence recoveries below 80% and whose sacrificial cores were not fully dissolved were not included. Data collected was then fitted using normalized first order rate kinetics and the $t_{1/2}$ (s) as well as rate constant were used to calculate diffusion coefficient, modeling 2D diffusion as follows:

$$D = \frac{\omega 2 \ln(2)}{4t1/2}$$

where D is the Diffusion coefficient in μm^2 s^{-1}, ω is the bleach spot radius in μm and *t½* is the fluorescence recovery half-life in seconds. FRAP measurements on the LA-PEM microcapsules were obtained with slight modifications to the above procedure as these systems required using SB dye as the diffusible probe, but lysine as the aptamer's target. FRAP was done on samples containing 3 μM L-lysine (0.1 M KCl) as target or 3 μM L-histidine (0.1MKCl) as a negative control with 100 μM SB dye as the fluorescent probe. Also, due to their reduced stability, the LA-microcapsules were imaged without annealing.

The effect of target binding on the integrity of the aptamer-loaded PEM microcapsules was examined by cryo SEM and CLSM. 1 μL of 6-FAM labeled aptamer microcapsule samples were incubated in 50 μL of either 1 mM SB in 0.1 M KCl or 10 μM SB in 0.1 M KCl solutions for up to 6 days. After incubation, all samples were centrifuged and washed three times with deionized water to remove the extra dye prior to microscopy. The capsules were also incubated in 1 mM TMR (in 0.1 M KCl) for 6 days to examine the specificity of the systems.

3. Results and discussion

3.1. General discussion of current systems

Polyelectrolyte multilayers (PEMs) can be prepared via layer-by-layer (LBL) assembly, which involves the sequential adsorption of oppositely charged polyelectrolytes onto a charged substrate. Each polyelectrolyte is negatively or positively charged, allowing for electrostatic interactions to hold the multilayer film together. PEM films and microcapsules are well-suited for the development of smart materials due to the nanoscale control of their film thickness and composition and the fact that they are compatible with almost any charged material, including nanoparticles and biomolecules. Given their negatively charged backbone, aptamers can be readily incorporated into these materials using LBL deposition methods. This provides an opportunity to prepare PEM films and microcapsules whose permeability or integrity can be altered in response to a molecular target. In the systems discussed in this paper and in the literature, it is the case that aptamers for small molecules are incorporated into the smart material. This is especially important if the aptamer is physically embedded within the PEM film or loaded within the microcapsule as PEMs have some intrinsic permeability to water and small molecules [24,25] allowing the target access to the aptamer. Table 1 lists the aptamer systems that have been incorporated into PEM films and microcapsules, and the new responsiveness that is observed in the system due to aptamer incorporation. The following sections provide some insight into the development of these aptamer-PEM smart materials, with considerations on the methods for their preparation, characterization, and testing.

Prior to a more in depth discussion on the different aptamer-PEM smart materials, some general considerations apply to all aptamer-PEM systems that warrant discussion. In terms of the DNA used for the materials, the aptamer of interest, as well as a random oligomer for use in control films, can be prepared in-house using a DNA synthesizer or purchased from a custom DNA synthesis company. Earlier work on aptamer-PEM systems also used CT DNA within the films as a control system. However, the large size difference between CT DNA and the oligonucleotides was found to lead to different morphologies in the films themselves, making the CT PEM films less appropriate for comparison [26]. Depending on the characterization methods chosen, the oligonucleotides could be prepared unmodified or tagged with an appropriate fluorophore for monitoring incorporation into the films. Purification by Reverse Phase HPLC or polyacrylamide gel electrophoresis is recommended and the molecular weight of the sequences should be confirmed by mass spectrometry. Also, some care should be taken to ensure that the oligonucleotides are prepared in such a way that allows them to fold into the proper structure for target binding. This could involve heating and cooling the aptamer sample in an appropriate buffer prior to deposition, or annealing the films or microcapsules after deposition, under conditions suitable for target binding. Some thought should be paid to the polyelectrolytes that are chosen for the smart material system. Polyelectrolytes can be sorted into two groups: those with permanent charges in solution (strong) and those whose charge depends strongly on pH (weak). Furthermore, PEs can be distinguished as those of synthetic origin or natural origin. Table 2 lists some examples of PEs that have been used in aptamer-based films or microcapsules, as well as other examples. The choice of strong vs weak polyelectrolyte could influence the film growth mechanism, with strong polyelectrolytes more likely to grow linearly with number of deposited bilayers, while weaker polyelectrolytes are known to grow exponentially, leading to island formation and discontinuities. In addition to the polymer's composition, the molecular

Table 1
List of aptamers that have been incorporated into PEM films and microcapsules. The application of the smart material system and the new responsiveness imparted by the aptamer are described.

Molecule detected	Application	Responsiveness	Reference
Sulforhodamine B (SB)	Films	~2× increase in target binding over control films	[14]
	Films	~2× increase in diffusion of a redox active probe over control films	[26]
	Microcapsules	~8× increase in diffusion of target over control microcapsules	[19]
	LSPR sensor	Est. 2× increase in diffusion of etchant over control films[1]	[16]
	Biodegradable films	~2× increase in target binding over control films	[18]
Quinine	LSPR sensor	Est. 4× increase in diffusion of etchant over control films[2]	[16]
Lysine	Microcapsules	~2× increase in diffusion of a fluorescent dye over control microcapsules	[26]
D-Arginine Vasopressin (D-VP)	Electrochemical sensor	LOD 1 ng/mL	[15]
Bisphenol A (BPA)	ECL sensor	Increased diffusion of a coreactant $S_2O_8^{2-}$ required for ECL, leading to a 64× increase in ECL intensity over control film; LOD 0.05 ng/mL	[17]

[1] Estimated from Fig. 2b from Malile et al. [16].
[2] Estimated from Fig. 4b from Malile et al. [16].

weight of the chosen system can influence the material's properties. While the growth rate is unaffected, using higher molecular weight polyelectrolytes causes a shift to exponential growth more quickly than smaller polyelectrolytes [27,28] and deposition of lower molecular weight polyelectrolytes has been shown to create rougher films [29].

While a variety of aptamers have been incorporated into polyelectrolyte multilayers (see Tables 1 and 2), the following sections will examine PEM films and microcapsules using either the sulforhodamine B aptamer (SA) or the lysine (LA) aptamer. Synthetic PEMs built from combinations of PDDA or PAH, and PSS will be described, along with natural PEMs prepared from CHI and HA. Methods to monitor film growth, structure, and functionality are described.

3.2. Preparation of aptamer-embedded PEM films

The choice of deposition conditions can impact a number of characteristics of the aptamer-PEM smart material. Film thickness, morphology, and permeability can all be altered depending on the deposition conditions, such as ionic strength, pH, and even the extent of inter-deposition rinsing. When considering the pH of the deposition solution, the nature of the polyelectrolyte and the stability of the aptamer needs to be taken into account. For example, with weak polyelectrolytes CHI and HA, the solutions needed to be slightly acidic in order to ensure that the systems were charged. However, because DNA is unstable under acidic conditions, a balance must be struck. Aptamer-PEM systems have been shown to be effective with deposition pHs as low as 4.5 [18]. Ionic strength can impact the mechanism of PEM film growth (linear vs. exponential) which can in turn impact film thickness and morphology of the resulting films. Typically, the growth of PEM films are more likely to be exponential when deposited at a higher ionic strength and more linear at decreased salt concentration [27]. The size and thickness of the islands have also been seen to decrease with lower ionic strength. Even the duration and volume of the rinses used during film deposition have been found to affect the growth dynamics, the distribution of DNA within the films, as well as the level of target binding to the films. In aptamer-embedded CHI/HA films, longer rinse times and volumes led to a transition from linear growth to exponential-like growth. These longer rinse times also led to a higher amount of non-specific dye retention within the films. Shorter rinse times led to linearly growing films showing higher aptamer-target binding and thus were preferred [18]. The length and structure of the aptamer sequence may also impact its deposition within PEM films. Using fluorescence microscopy to compare 6-FAM tagged SA vs. 6-FAM tagged RO embedded within CHI/HA films, it was evident by the dramatically brighter signal that RO DNA was more easily loaded into the films than SA DNA, an indication that the DNA structure may play a role in its deposition. The SA DNA forms a structured G-quadruplex, while the RO DNA does not. This could allow the RO DNA a looser, extended conformation, giving it more interaction with the polyelectrolyte layers [38].

Table 2
Some examples of weak and strong polyelectrolytes commonly used in literature. Polymers highlighted with a * have been employed in aptamer-PEM systems.

Weak PEs	Reference
Chitosan (CHI)*	[18,30]
Poly(allylamine hydrochloride) (PAH)*	[19,30]
Poly(acrylic acid) (PAA)	[30]
Poly(ethylene oxide) (PEO)	[31]
Poly(methyl methacrylate) (PMMA)	[31]
Polyethyleneimine (PEI)*	[17,32]
Poly(L-lysine hydrochloride) (PLL)	[33]
Hyaluronic acid (HA)*	[18,33]
Poly-2-vinyl pyridine (PVP)	[34,35]
Strong PEs	**Reference**
Poly(sodium-p-styrenesulfonate) (PSS)*	[14,32,36]
Poly(diallyldimethylammonium chloride) (PDDA)*	[14,37]

As so many factors affect the resulting PEMs, whenever possible it is advisable to monitor the progress of the deposition process. Depending on the polyelectrolytes used and the substrate for the deposition, there are a number of techniques that provide a great deal of information about the development of the PEM film. Building the PEM films on glass or quartz slides allows for the examination of multilayer growth by UV–Vis [14,16,18]. For example, the growth of the PDDA/PSS films could be monitored after the addition of each bilayer by observing the absorbance of PSS around 220 nm. The growth of the CHI/HA films was monitored via the absorbance of glucosamine and N-acetylglucosamine between 190 and 220 nm. When DNA was used as the negative PE, the growth can also be monitored at 260 nm. Fig. 4a shows some representative spectra from the deposition of a multilayer of CHI/HA. Other spectroscopic approaches such as fluorescence spectroscopy and IR spectroscopy could also be used to track the deposition of fluorescent polyelectrolytes, or those containing functional groups with strong, characteristic IR-active vibrations, respectively. PEM film depositions on an electrode surface can easily be monitored by electrochemical methods, such as impedance spectroscopy [17] or cyclic voltammetry [26]. For example, the peak current of a redox active probe in solution should decrease as the thickness of the PEM film on the electrode surface increases. Fig. 4b shows a representative series of cyclic voltammograms where the signal

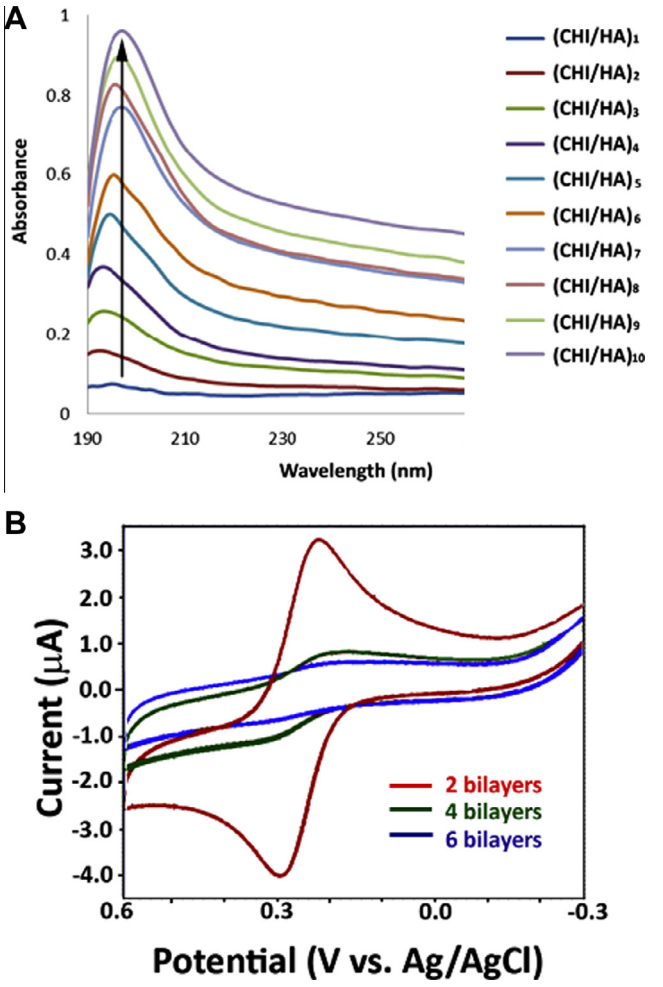

Fig. 4. Example methods for monitoring bilayer deposition during LBL film preparations. (A) UV–vis spectra showing the growth of the absorbance band at approximately 200 nm with deposition of CHI/HA bilayers. Modified from reference [18]. (B) Cyclic voltammograms showing the reduction in peak current for the redox probe ferricyanide with increasing PAH/PSS bilayers deposited on a Au electrode surface [26].

from a redox active probe (ferricyanide) decreases as the number of deposited bilayers is increased. Other techniques such as QCM can track the increase in mass deposited on the surface of a quartz crystal, while zeta potential measurements can confirm the change in surface charge as a result of the deposition of the polyelectrolytes [14,20]. The disadvantage of electrochemical techniques or mass-based techniques such as QCM is that they can only report on changes at the surface, without providing information about the composition of the materials making those changes. For this reason, spectroscopic approaches are particularly useful when probing the deposition process.

Once deposited, the thickness and morphology of the aptamer-PEM films can be confirmed using microscopy techniques, such as SEM and AFM, while composition can be verified by fluorescence microscopy, CLSM, and profiling techniques such as ToF-SIMS. Different polyelectrolyte combinations can be expected to yield PEM films with different properties, which will impact their effectiveness as smart materials. For example, in the PDDA/PSS family of aptamer-embedded PEMs, SEM was used to confirm that deposition yielded a smooth continuous base for the aptamer-containing bilayer after only five bilayers, while CHI/HA films only showed the formation of continuous films by SEM after 10 bilayers. Due to the island growth mechanism of the aptamer-embedded CHI/HA films, AFM confirmed that they were continuous, but much rougher than the PDDA/PSS films [18].

By tracking secondary ions that are unique to the polyelectrolyte of interest, a profiling method such as ToF-SIMS analysis can provide a depth profile of the films to confirm their composition. This method was particularly effective in the case of aptamer-embedded PDDA/PSS systems [14]. DNA layers were tracked by following the PO_3^- ion, while the PSS layers were monitored by following the SO_2^- ion. As the two negatively charged polyelectrolytes were spatially separated within the PEM, the depth profile showed SO_2^- ion from the PSS layers diminishing when the PO_3^- ion from the DNA layers was increasing. The PDDA/PSS films grew linearly, allowing the depth profile determined by the ToF-SIMS to distinguish specific layers in the films that were clearly defined. In the aptamer-embedded CHI/HA biodegradable films, however, the growth of the PEM was exponential, leading to the diffusion of each polyelectrolyte into multiple layers resulting in a film with less structure and without distinct layers. This led to a ToF-SIMS depth profile that lacked the distinct regions of the polyelectrolytes. Nevertheless, ToF-SIMS did confirm the presence of the expected secondary ions (PO_3^{3-} or PO_2^{2-} for DNA and CHO_2^- from the CHI/HA matrix) and thus helped to confirm the PEM composition [38].

3.3. Characterization of aptamer-PEM film target binding and responsiveness

The ability of an aptamer to fold into its unique secondary structure that allows for target binding is critical for the efficacy of any aptamer-based smart material. Given that the electrostatic interactions of an aptamer within a PEM could interfere with aptamer folding and, consequently, target binding, it is critical to assess aptamer affinity and specificity once it is embedded within the PEM matrix. The effects of the polyelectrolyte film on target recognition and binding could be studied with a variety of techniques, including UV–Vis, ToF-SIMS, fluorescent microscopy, and electrochemistry.

The SA system that has been used in several aptamer-PEMs is known to form a G-quadruplex structure that requires K^+ for effective binding [39]. Given that the target molecule, SB, is a fluorescent dye, absorbance and/or fluorescence spectroscopy can be used to determine the extent of target binding by the film. For example, in the PDDA/PSS family of PEMs, the absorbance of SB at 570 nm for the aptamer-embedded films, in the presence and absence of K^+, was compared to that of control films [14]. The ratio of dye peak height to DNA peak height (at 260 nm) was used for comparison to account for any differences in the DNA loading within the films. Since the SB dye is negatively charged, some non-specific electrostatic interactions with the films were expected. Fig. 5a shows the results of this comparison. Films containing CT or RO DNA gave ratios of 0.23 ± 0.02 and 0.34 ± 0.09, respectively. Without K^+, the dye to DNA ratio was similar to the control level with a ratio of 0.26 ± 0.03. When exposed to SB in the presence of K^+, however, the ratio jumps to 0.70 ± 0.01, indicative of the aptamer's ability to form a G-quadruplex in the presence of K^+ and bind its target even while embedded in the PEM film. When exposed to the structural analog TMR, the PDDA/PSS/SA films showed the low dye to DNA ratio of 0.17 indicating that the SA aptamer not only retains its binding abilities within the polyelectrolyte film, but also its specificity. A more complete analysis of binding by determining the dissociation constant of the SA aptamer in the film was investigated also using UV–Vis, by monitoring the change in absorbance at 570 nm over a range of SB concentrations [14].

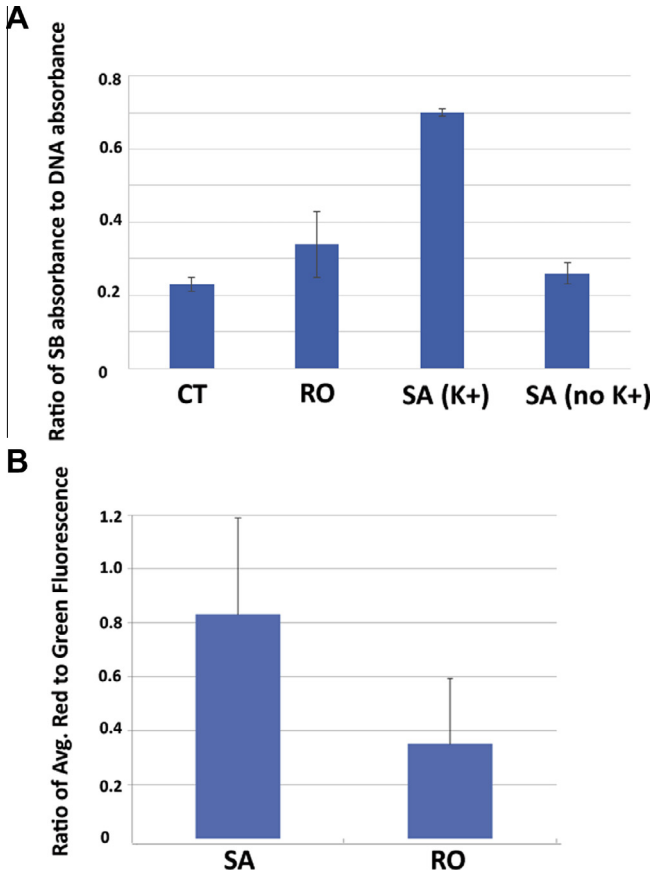

Fig. 5. Examination of target binding in PEM films. (A) Ratio of the UV–vis absorbance of SB dye (570 nm) to the absorbance of DNA (260 nm), for a series of SA-embedded PDDA/PSS PEM films and controls. The films were exposed to 2 mM SB dye in either the absence or presence of K^+, which is required for target binding. In the absence of K^+, the SA-embedded film shows no increase in target binding over the controls. In the presence of K^+, 2× better target binding is observed in the SA-embedded films. Each ratio represents the average of at least 3 measurements, and the standard deviation is shown as error bars. Modified from [14]. (B) Ratio of SB fluorescence to 6-FAM fluorescence for measuring colocalization of either SA or RO with the SB target within CHI/HA films. A significantly higher ratio was observed for the SA-embedded films ($p = 0.0008$, $\alpha = 0.05$) than the RO-embedded films, indicative of specific target binding within the aptamer-embedded films. Modified from reference [18].

Other techniques can provide valuable information with regards to aptamer-target binding. QCM can be used to measure the small changes in the mass of the film due to target binding. For example, the K_d of SA within PDDA/PSS PEM films was determined using QCM on the quartz crystal, measuring changes in frequency over a range of SB concentrations, and this was compared to CT-embedded PDDA/PSS films. Using this method, it was confirmed that the data fit a model with two binding affinities: a specific K_d of 16 μM associated with aptamer-target binding, and a non-specific K_d of 1.5 mM representing the dye interacting with the film. This result indicated that the aptamer retains its binding affinity within the film, exhibiting only a minor loss in affinity (~20×) [14].

ToF-SIMS can also be used to measure the binding ability of the aptamer within the PEMs by confirming the presence of secondary ions associated with the target within the film. Furthermore, a depth profile of the films can allow for aptamer-target colocalization to be studied in films with well-defined bilayers such as the PDDA/PSS system [14]. After incubation of SB with the SA-embedded PDDA/PSS films, the secondary ions associated with the target dye was found among the layers of aptamer within the film and not within polyelectrolyte layers, indicative of specific aptamer-target binding. Unfortunately, this technique is not applicable to all aptamer-PEM films. Target binding in the aptamer-embedded CHI/HA system, with less structure and without distinct layers, was more difficult to monitor by ToF-SIMS [38]. While the expected secondary ion (SO_3^{2-} from the SB dye) was present within the films, and more SB was retained in the aptamer-embedded film than in the random oligonucleotide film, it was not possible to confirm colocalization with the aptamer containing layer.

In the smart material systems where the target molecule is fluorescent, fluorescence microscopy or CLSM can be employed to confirm target binding to the film, as well as colocalization with the aptamer when fluorophore-tagged aptamers are used. For example, CLSM has been employed to compare the levels of SB dye binding in aptamer-embedded PDDA/PSS films and controls [14]. The SA films showed high levels of bright spots, indicating that clusters of aptamers were binding the target dye. The fluorescence of all the films was analyzed using photo processing software, and it was found that the mean brightness of the aptamer films was 2× higher than films containing RO, and 30× higher than those prepared with CT. For CHI/HA films, fluorescence microscopy allowed for the examination of dye binding [18]. Greater dye binding was observed in the SA-embedded CHI/HA films compared to the RO films. While colocalization of aptamer and SB dye in the CHI/HA films was not observed using ToF-SIMS because of the many peaks and valleys in each film, colocalization experiments could be performed using fluorescence microscopy. Using the mean fluorescence values from each channel, ImageJ software was used to calculate the ratio of dye signal to the signal for the 6-FAM-tagged DNA. This ratio was significantly higher for the SA-embedded films ($p = 0.0008$, $\alpha = 0.05$) than the RO-embedded films. (See Fig. 5b).

As aptamer structure is critical to interactions with its target, it is important to consider whether annealing the PEM films after deposition (the heating and slow cooling of the film to ensure proper aptamer folding) has an impact on target binding. The annealing process was found to be important for aptamer-target binding in the synthetic PDDA/PSS film system [14], while in the CHI/HA film system it increased non-specific binding [18]. The PDDA/PSS films are deposited as distinct layers of oppositely charged polyelectrolytes which interact with the layers above and below. These electrostatic interactions could interfere with the proper folding of the aptamer, in which case the annealing process could aid in its ability to properly fold. With the more exponential-like growth of CHI/HA systems, the polyelectrolytes are not formed in distinct layers, and the annealing may allow loosely associated polyelectrolytes to escape the film, allowing more dye to penetrate the looser structure. In cases such as these, extra care should be taken to ensure proper folding of the aptamer prior to deposition. Nevertheless, there should be no obvious impediment to the choice of either class of polyelectrolyte (synthetic vs. natural) for use in aptamer-enabled applications.

While simple target binding is sufficient for aptamer-PEM films that will be employed for direct sensing, smart material applications may require a different level of responsiveness of the film to the target molecule. For example, the effect of target binding on the permeability of the film could be important for targeted delivery applications where detection of the target leads to the release of a payload. Permeability can be investigated by depositing the aptamer-PEM film on an electrode surface and measuring any changes in diffusion of a redox-active probe through the films once target is introduced. For example, Fig. 6 shows the results of an experiment with SA-embedded PAH/PSS PEM films. A comparison of several films deposited on gold electrodes included a polyelectrolyte film with no DNA, $(PAH/PSS)_4$, a film with a random oligonucleotide as control DNA, $(PAH)_4(RO)_2(PSS)_2$ and a film

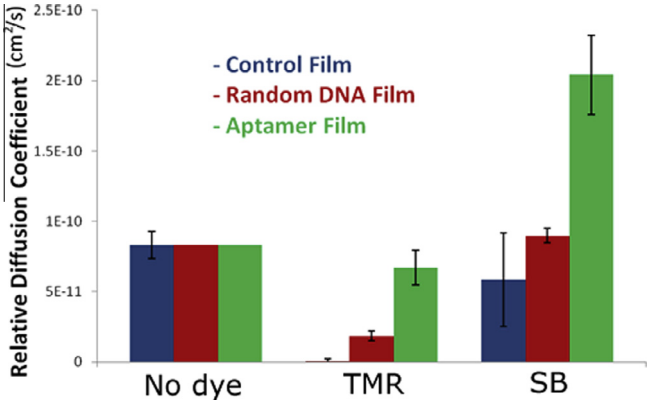

Fig. 6. Comparison of the permeability of PEMs to a redox active probe. Three film types were examined ($n = 3$ for each): a film containing only PAH/PSS (blue), SA-embedded PAH/PSS (green) and RO-embedded PAH/PSS (red). The diffusion coefficient for $[Ru(NH_3)_6]^{3+/2+}$ was measured under three conditions for each film: without any target molecule present (no dye), in the presence of the non-specific molecule TMR (TMR) and in the presence of the aptamer's target (SB). All coefficients were normalized to the values measured under "no dye" conditions. A 2× increase in diffusion coefficient was observed only in the case where the aptamer film was exposed to its target.

containing the aptamer, $(PAH/SA)_2(PAH/PSS)_2$. The permeability of the redox active probe, $[Ru(NH_3)_6]^{3+/2+}$, through these three films was examined under three conditions: in the absence of any target molecule, in the presence of TMR, and the presence in of SB. A statistically significant increase in diffusion ($p = 0.009–0.02$) was seen in the SA film after target addition over either of the control films in the presence of SB. No increase in diffusion is observed when TMR was used instead of target, confirming the specificity of the film's permeability changes [14].

3.4. Preparation of aptamer-embedded PEM microcapsules and aptamer-loaded PEM microcapsules

Just as polyelectrolyte films are created by LBL assembly described in Section 3.1, microcapsules can be built in the same manner by the sequential addition of oppositely charged polymers, in this case onto a sacrificial spherical template. Polyelectrolyte microcapsules have been of interest for applications such as triggered delivery systems for a molecular payload. The two main payload release strategies that have been explored involve either release which stems from stimuli-triggered changes in the permeability of the capsule coating or release which is dependent on stimuli-triggered decomposition of the microcapsule [40–44]. Variations on both approaches have been attempted with aptamer PEM systems. In this section, methods for the fabrication of microcapsules with aptamers embedded in their polyelectrolyte wall (aptamer-embedded microcapsules) or within their core (aptamer-loaded microcapsules) will be described. Systems based on SA or LA have been investigated.

The first step in the preparation of aptamer-PEM microcapsules is the formation of the sacrificial template upon which the PEM and aptamer will be deposited. The nature of this template will depend on your application. For the aptamer-based systems, spherical calcium carbonate particles have been used as a template. These particles can be prepared either doped with the aptamer of interest (for the preparation of aptamer-loaded PEM microcapsules) or not (for aptamer-embedded PEM microcapsules). Depending on whether or not aptamer-doping is required, as well as on the nature of the aptamer being loaded in the spheres, existing protocols for the preparation of spherical calcium carbonate particles [45,46] may need to be modified. It was found that careful control over a variety of parameters was crucial to ensure an acceptable yield of spherical particles over the cubic form. Interestingly, it was discovered that the stirring speed had a direct effect on the morphology of microstructures formed as slower stirring speeds resulted in cubic crystallization as compared to spherical structures obtained at higher speeds [26]. See Fig. 7a and b. Other parameters such as Ca^{2+} concentration, temperature, and reaction time can impact the yield of spherical particles. For aptamer-loaded particles, the ratio of DNA to Ca^{2+} also needed to be optimized to ensure that the aptamer was distributed inside

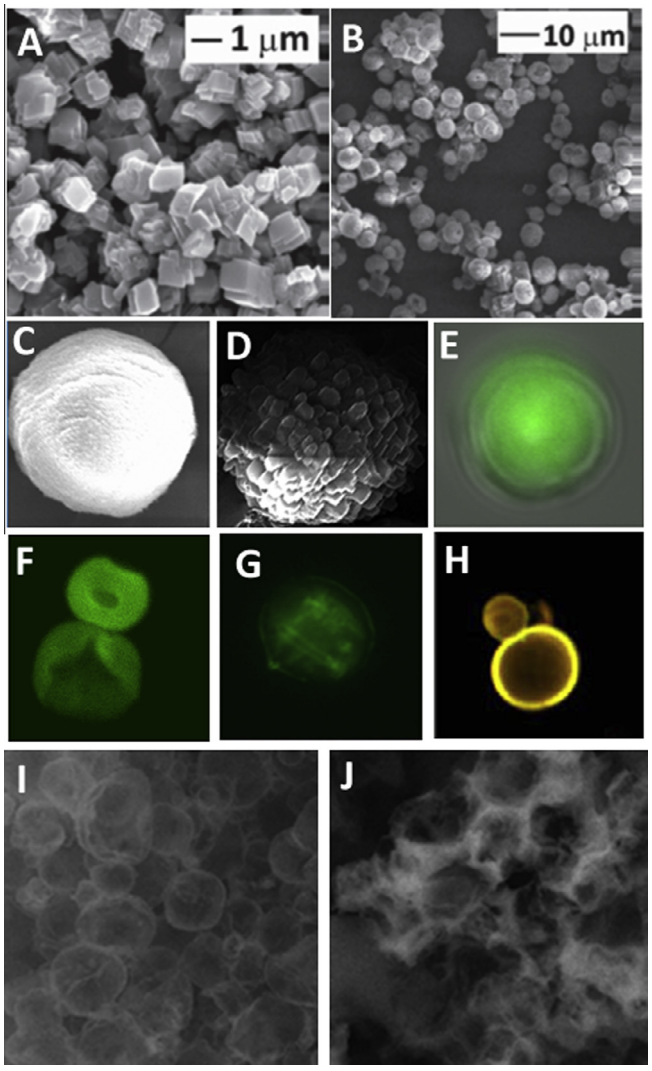

Fig. 7. SEM and CLSM images for characterization of aptamer-embedded and aptamer-loaded PEM microcapsules. (A) SEM image of a failed attempt to prepare spherical calcium carbonate template particles under conditions where stirring was too slow. (B) SEM image of a successful batch of calcium carbonate particles. (C) Image of a PSS-doped calcium carbonate particle prior to deposition. (D) SEM image after the deposition of one polyelectrolyte later. (E) CLSM image showing the fluorescence from 6-FAM labeled aptamer loaded into a calcium carbonate core. (F) Hollow 6-FAM aptamer-embedded PAH/PDDA microcapsules after template dissolution. The strong green fluorescence in the wall of the microcapsule is an indication of successful aptamer incorporation. (G) CLSM image of a 6-FAM aptamer-loaded PAH/PSS microcapsule after template dissolution. The green color associated with the aptamer is localized within the center of the microcapsule and not within the wall. (H) Aptamer-target binding is confirmed by a CLSM study showing the overlay of the green color of 6-FAM SA colocalized with the red color of the SB target to yield a bright yellow color within the wall of the aptamer-embedded microcapsule. (I) Cryo SEM image of SA-loaded PDDA/PSS microcapsules after incubation in 10 μM SB for six days. (J) Cryo SEM image of ruptures SA-loaded microcapsules after incubation in 3 mM SB for six days.

the $CaCO_3$ particle [20]. SEM, EDX, CLSM, and zeta potential measurements can provide important information about the morphology, size, and composition of the templates. For example, SEM with EDX has been used to confirm the presence of phosphorus from the aptamer within the spherical templates. The fluorescence signal from 6-FAM-tagged SA has been examined by CLSM to confirm aptamer loading into the particles. (Fig. 7e) Zeta potential measurements also corroborate that the aptamer has been taken up into the templates. The zeta potential of undoped calcium carbonate cores dispersed in distilled water were found to have a Zeta potential of +12.5 mV. However, a drop of zeta potential to a −22.3 mV was measured after SA aptamers were loaded into the $CaCO_3$ particles, consistent with the incorporation of the negatively charged biomolecule. (See Table 3).

Once the templates are prepared and well-characterized, depositions to prepare the PEM-microcapsules should be monitored just as was the case for the PEM-films. While the presence of the $CaCO_3$ particle makes it somewhat more difficult to monitor deposition, there are some effective approaches available. Zeta potential measurements can be used to inform conditions for PEM deposition. For example, Table 3 lists zeta potentials that were recorded for PEM depositions on $CaCO_3$ particles under different polyelectrolyte concentrations. The zeta potential for the negatively charged particles after deposition of the first positively charged PAH layer (either 2 mg/mL or 3 mg/mL) were both positive at 4.0 mV and 3.5 mV, respectively. The positive surface charge is a good indication of successful deposition of PAH onto the aptamer-calcium carbonate core surface. However, the value measured was lower than that typically observed (40 mV) for PAH outermost layer in hollow microcapsules [47]. This observation can be explained by the loading of the negatively charged aptamer inside the calcium carbonate which can partially neutralize the positively charged PAH [45]). When the particles were incubated in PSS solution, again either 2 mg/mL or 3 mg/mL, the zeta potentials were found to be −0.7 mV and −18.5 mV, respectively, suggesting that the higher concentrations of the PAH and PSS led to more complete bilayer deposition. Other considerations to make when designing the deposition procedure include the total number of bilayers to be added to the cores. The extent of polyelectrolyte aggregation (agglomeration of polyelectrolytes unassociated to the template) increases as the number of bilayers increases. On the other hand, microcapsules made of too few bilayers become unstable and often collapse and burst during core dissolution. Doping of even the aptamer-free calcium carbonate particles with a small amount of PSS was found to improve the stability of the resultant microcapsules after PEM deposition and core dissolution. The hypothesis is that the PSS, after core dissolution, serves as a structural support for the PEM microcapsule wall. In fact, it was based on this concept that the idea for the aptamer-loaded microcapsules emerged; after dissolution of the core, aptamers could serve as a scaffold for supporting the PEM wall, until target binding (see Fig. 3). Once again, SEM and CLSM can also be used to monitor PEM microcapsule preparation. By SEM, the roughness of the spherical templates can be seen to increase as depositions progress. (See Fig. 7c and d) If 6-FAM labeled aptamers are used, their presence on the surface of the coated templates can be confirmed by CLSM.

Once deposition of oppositely charged polyelectrolytes is complete, the template is dissolved to yield the aptamer-embedded or the aptamer-loaded microcapsule. Following complete surface coverage by a specific polyelectrolyte, samples should be centrifuged and extensively washed to ensure that unbound polyelectrolyte has been removed. To confirm that the microcapsules are intact after core dissolution, SEM with EDX, as well as cryo-SEM with the hydrated microcapsules, are informative techniques that can be employed. The location of the aptamer within the microcapsules can be determined by the presence of phosphorus by EDX as well as the 6-FAM fluorescence signal by CLSM in tagged-aptamer microcapsules. Fig. 7f and g compares CLSM images from 6-FAM SA-embedded and 6-FAM SA-loaded PAH/PSS microcapsules respectively. Notably, deposition conditions that yield stable aptamer-embedded microcapsules with one aptamer may need to be modified when switching aptamers. LA-PAH/PSS microcapsules prepared under the same conditions as SA-PAH/PSS microcapsules were found to collapse and burst during template dissolution. LA, whose sequence is three times larger than SA, could experience greater flexibility or perhaps less efficient deposition. Increasing salt concentration to 0.8 M NaCl improved the stability of the LA-PEM microcapsules [26] potentially by increasing film thickness [48] of PAH and PSS onto the cores, ultimately providing more rigidity to the overall structure.

3.5. Characterization of target binding and responsiveness in aptamer-embedded and aptamer-loaded PEM microcapsules

Just as was described for the PEM-films, it is important to confirm the activity of embedded and loaded aptamers within the microcapsule environment. When the target is fluorescent, this can be achieved using CLSM and examining fluorescence colocalization. CLSM experiments with 6-FAM SA-embedded PAH/PSS systems once again confirmed the need for K^+ to ensure target binding; colocalization between the 6-FAM signal and the SB signal could be seen in SA-embedded samples but only when the samples were incubated in K^+ [19].

In addition to the ability to simply bind the target, the ability to translate that binding event into a change in the permeability or integrity of the microcapsule wall would allow for the preparation of smart materials for targeted delivery applications. Measurements of diffusion constant for the movement of SB through a series of microcapsules were achieved using Fluorescence Recovery after Photobleaching (FRAP). The technique, associated with CLSM, works by photobleaching the dye found inside a microcapsule and measuring the recovery of the signal as a result of the photobleached dye diffusing out of the capsule and new dye diffusing in. The FRAP results for SB diffusion through PAH/PSS microcapsules, RO-embedded PAH/PSS microcapsules, and SA-embedded microcapsules are shown in Fig. 8 (blue bars). Analyses of the diffusion coefficients indicate that the diffusion of the SB target molecule increases by 8× through SA-embedded PAH/PSS microcapsule over the controls. The red bars in Fig. 8 represent the diffusion of SB through LA-embedded PAH/PSS microcapsules in the presence of LA's target lysine, or a non-specific molecule, histidine. Interestingly, the LA-microcapsules become 2× more permeable to SB in the presence of lysine, in comparison to their response in the presence of histidine. These data confirm that effects of aptamer-target binding on permeability are applicable to other small molecules moving across the microcapsule wall and are not reserved simply for the aptamer's target. This has important implications for the use of aptamer-PEM microcapsules as smart materials for delivery applications; the aptamer-target binding event facilitates a general

Table 3
Zeta potential of undoped $CaCO_3$ templates, SA:PSS-$CaCO_3$ and PEM coated SA:PSS-$CaCO_3$ under different conditions.

Sample	Zeta potential (mV)
$CaCO_3$ particles	12.5
SA:PSS-$CaCO_3$ particles	−22.3
SA:PSS-$CaCO_3$ coated in 2 mg/mL PAH in 0.5 M NaCl	4.0
SA:PSS-$CaCO_3$ coated in 3 mg/mL PAH in 0.5 M NaCl	3.5
SA:PSS-$CaCO_3$ coated in 2 mg/mL PAH and 2 mg/mL PSS	−0.7
SA:PSS-$CaCO_3$ coated in 3 mg/mL PAH and 3 mg/mL PSS	−18.5

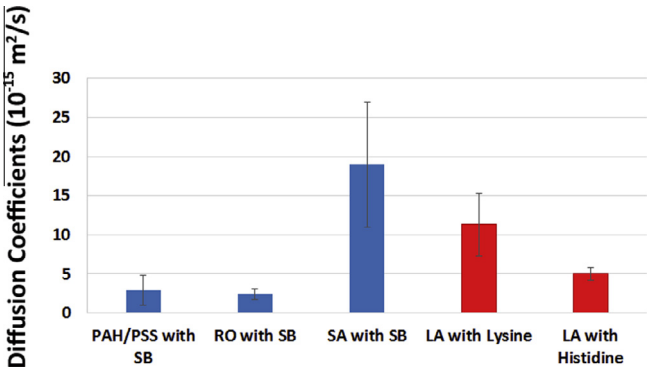

Fig. 8. Data from FRAP experiments measuring the diffusion of SB across the walls of two families of aptamer-embedded PAH/PSS microcapsules. The blue bars represent the results of the SA-embedded PAH/PSS microcapsules and controls (RO-embedded microcapsules and microcapsules composed of only the polyelectrolytes). The diffusion coefficient for SB is ~8× higher than the controls. The red bars represent the results of LA-embedded PAH/PSS microcapsules in the presence of lysine and a non-specific target, histidine. In this case, the diffusion of SB is 2× increased in the LA-microcapsules when they are exposed to the proper target [19,26].

increase in permeability in the microcapsule wall that could be used to trigger the release of a molecular payload. These data are also in agreement with the findings from the electrochemical study of the aptamer-PEM films.

It should be noted that accurate FRAP results are dependent on complete dissolution of the $CaCO_3$ templates. Using lower concentrations of EDTA for dissolution of calcium carbonate cores results in partial or incomplete removal of sacrificial cores which in turn impedes complete fluorescence intensity recovery after photobleaching [19]. Furthermore, the correct folding of the aptamer is critical to the responsiveness of the microcapsule system; 30% less permeability was noted for the SA-embedded PAH/PSS microcapsules when they were tested prior to annealing [19]. The LA-embedded PAH/PSS microcapsules proved to be less stable than their SA-based counterparts, thus they were tested without annealing, which may account for the lower responsiveness to target binding.

Aptamer-loaded PEM-microcapsule systems are based on a different mechanism for target-induced payload release. Upon the binding of the aptamer with its cognate target, a conformational change within the enveloped aptamer may interfere with its ability to serve as a scaffold to support the microcapsule wall, triggering the collapse of the microcapsules. CLSM can be used to monitor these changes in microcapsules loaded with 6-FAM-tagged aptamer. After 6 days in the presence of 10 mM target, only polymer debris and broken microcapsules could be seen by CLSM, while 6 days with the same concentration of TMR led to very little change to the microcapsule structures. Cryo SEM can also be used to track these target-induced morphological changes. Different target concentration (1 mM and 10 μM) and incubation time (16 h, 1 day and 6 days) were used to investigate the sensitivity and specificity of the microcapsule response. Cryo stage SEM experiments allow for the observation of microcapsule structure with the capsules hydrated, allowing for a clearer view of whether the microcapsules are burst or intact. At target concentrations above the aptamer-target dissociation constant (1 mM) the majority of the SA-loaded microcapsules have collapsed after 6 days (Fig. 7j). At very dilute SB concentrations (10 μM), however, the microcapsules are stable over this period of time. (Fig. 7i) Furthermore, the microcapsules are stable to 6 days incubation in 1 mM of the non-target molecule, TMR, confirming the specificity of the response.

4. Conclusions and future directions

Recent studies have confirmed that aptamer systems are able to largely retain their specific target binding functionality when incorporated into PEM-based materials. PEMs provide a flexible matrix that allow for aptamer folding and that respond to target binding. These unique responsive properties, coupled with the relative ease with which these materials can be prepared and characterized, has led to heightened interest in the application of these systems in biosensing and controlled delivery. Future efforts should include more extensive testing of aptamer incorporation into new polyelectrolyte systems, in particular those of natural origin that are most biocompatible and biodegradable. Furthermore, the limits of these systems in terms of the size of the payloads and the targets that can be employed, should be investigated. Current work has demonstrated that small molecule targets are able to effectively reach the aptamer to trigger an effect in the PEM film or microcapsule. Examination of larger target molecules could greatly expand the applicability of this approach.

Acknowledgements

The authors acknowledge the Natural Sciences and Engineering Council (NSERC), Canada Foundation for Innovation, Alberta Innovates Bio Solutions, the Ontario Ministry of Research and Innovation, and Carleton University for financial support.

References

[1] I. Roy, M.N. Gupta, Smart polymeric materials: emerging biochemical applications, Chem. Biol. 10 (2003) 1161–1171, http://dx.doi.org/10.1016/j.
[2] E. Mastronardi, A. Foster, X. Zhang, M.C. DeRosa, Smart materials based on DNA aptamers: taking aptasensing to the next level, Sensors (Basel) 14 (2014) 3156–3171, http://dx.doi.org/10.3390/s140203156.
[3] H. Yang, H. Liu, H. Kang, W. Tan, Engineering target-responsive hydrogels based on aptamer-target interactions, J. Am. Chem. Soc. 130 (2008) 6320–6321, http://dx.doi.org/10.1021/ja801339w.
[4] F. El-Hamed, N. Dave, J. Liu, Stimuli-responsive releasing of gold nanoparticles and liposomes from aptamer-functionalized hydrogels, Nanotechnology 22 (2011) 494011, http://dx.doi.org/10.1088/0957-4484/22/49/494011.
[5] X. He, B. Wei, Y. Mi, Aptamer based reversible DNA induced hydrogel system for molecular recognition and separation, Chem. Commun. (Camb.) 46 (2010) 6308–6310, http://dx.doi.org/10.1039/c0cc01392g.
[6] B.-C. Yin, B.-C. Ye, H. Wang, Z. Zhu, W. Tan, Colorimetric logic gates based on aptamer-crosslinked hydrogels, Chem. Commun. 48 (2012) 1248, http://dx.doi.org/10.1039/c1cc15639j.
[7] H. Zhang, Y. Ma, Y. Xie, Y. An, Y. Huang, Z. Zhu, C.J. Yang, A controllable aptamer-based self-assembled DNA dendrimer for high affinity targeting, bioimaging and drug delivery, Sci. Rep. 5 (2015) 10099.
[8] G. Decher, Fuzzy nanoassemblies: toward layered polymeric multicomposites, Science 277 (1997) 1232–1237, http://dx.doi.org/10.1126/science.277.5330.1232 (80-).
[9] V.S. Goudar, S. Suran, G.R. Prashanth, M.M. Varma, Detection of hepatitis B DNA sequences on polyelectrolyte based non-covalently functionalized flexible plastic substrates, IEEE Sens. J. 13 (2013) 4817–4823.
[10] E.M. Saurer, C.M. Jewell, D.A. Roenneburg, S.L. Bechler, J.R. Torrealba, T.A. Hacker, et al., Polyelectrolyte multilayers promote stent-mediated delivery of DNA to vascular tissue, Biomacromolecules 14 (2013) 1696–1704, http://dx.doi.org/10.1021/bm4005222.
[11] W.W. Hu, S.L. Tsou, The effect of alginate on DNA delivery from layer-by-layer assembled films, Carbohydr. Polym. 101 (2014) 240–248, http://dx.doi.org/10.1016/j.carbpol.2013.09.025.
[12] W. Teng, Q. Wang, Y. Chen, Controllably local gene delivery mediated by polyelectrolyte multilayer films assembled from gene-loaded nanopolymersomes and hyaluronic acid, Int. J. Nanomed. (2014) 5013–5024.
[13] Y. Zou, L. Xie, S. Carroll, M. Muniz, H. Gibson, W.-Z. Wei, et al., Layer-by-layer films with bioreducible and nonbioreducible polycations for sequential DNA release, Biomacromolecules 15 (2014) 3965–3975, http://dx.doi.org/10.1021/bm5010433.
[14] Y. Sultan, R. Walsh, C. Monreal, M.C. DeRosa, Preparation of functional aptamer films using layer-by-layer self-assembly, Biomacromolecules 10 (2009) 1149–1154, http://dx.doi.org/10.1021/bm8014126.
[15] H. Qin, J. Liu, C. Chen, J. Wang, E. Wang, An electrochemical aptasensor for chiral peptide detection using layer-by-layer assembly of polyelectrolyte-methylene blue/polyelectrolyte-graphene multilayer, Anal. Chim. Acta 712 (2012) 127–131, http://dx.doi.org/10.1016/j.aca.2011.10.044.

[16] B. Malile, J.I.L. Chen, Morphology-based plasmonic nanoparticle sensors: controlling etching kinetics with target-responsive permeability gate, J. Am. Chem. Soc. 135 (2013) 16042–16045, http://dx.doi.org/10.1021/ja4086269.
[17] L. Chen, X. Zeng, A.R. Ferhan, Y. Chi, D.-H. Kim, G. Chen, Signal-on electrochemiluminescent aptasensors based on target controlled permeable films, Chem. Commun. 51 (2015) 1035–1038, http://dx.doi.org/10.1039/C4CC07699K.
[18] A. Foster, M.C. DeRosa, Development of a biocompatible layer-by-layer film system using aptamer technology for smart material applications, Polymers (Basel) 6 (2014) 1631–1654, http://dx.doi.org/10.3390/polym6051631.
[19] Y. Sultan, M.C. DeRosa, Target binding influences permeability in aptamer-polyelectrolyte microcapsules, Small 7 (2011) 1219–1226, http://dx.doi.org/10.1002/smll.201001829.
[20] X. Zhang, D. Chabot, Y. Sultan, C. Monreal, M.C. DeRosa, Target-molecule-triggered rupture of aptamer-encapsulated polyelectrolyte microcapsules, ACS Appl. Mater. Interfaces 5 (2013) 5500–5507, http://dx.doi.org/10.1021/am400668q.
[21] Y. Zhao, L.-P. Lv, S. Jiang, K. Landfester, D. Crespy, Advanced stimuli-responsive polymer nanocapsules with enhanced capabilities for payloads delivery, Polym. Chem. 6 (2015) 4197–4205, http://dx.doi.org/10.1039/C5PY00323G.
[22] S.L. Beaucage, R.P. Iyer, Advances in the synthesis of oligonucleotides by the phosphoramidite approach, Tetrahedron 48 (1992) 2223–2311, http://dx.doi.org/10.1016/S0040-4020(01)88752-4.
[23] A. Voigt, H. Lichtenfeld, G.B. Sukhorukov, H. Zastrow, E. Donath, H. Ba, et al., Membrane filtration for microencapsulation and microcapsules fabrication by layer-by-layer polyelectrolyte adsorption, Ind. Eng. Chem. Res. 38 (1999) 4037–4043, http://dx.doi.org/10.1021/ie9900925.
[24] K. Glinel, M. Prevot, R. Krustev, G.B. Sukhorukov, A.M. Jonas, H. Möhwald, Control of the water permeability of polyelectrolyte multilayers by deposition of charged paraffin particles, Langmuir 20 (2004) 4898–4902, http://dx.doi.org/10.1021/la036078l.
[25] A.E. El Haitami, D. Martel, V. Ball, H.C. Nguyen, E. Gonthier, P. Labbe, et al., Effect of the supporting electrolyte anion on the thickness of PSS/PAH multilayer films and on their permeability to an electroactive probe, Langmuir 25 (2009) 2282–2289.
[26] Y. Sultan, Development of Smart Materials Using Aptamer Based Bionanotechnologies, 2011.
[27] L. Richert, P. Lavalle, E. Payan, X.Z. Shu, G.D. Prestwich, J. Stoltz, et al., Layer by layer buildup of polysaccharide films: physical chemistry and cellular adhesion aspects layer by layer buildup of polysaccharide films: physical chemistry and cellular adhesion aspects, Langmuir 20 (2004) 448–458, http://dx.doi.org/10.1021/la035415n.
[28] C. Porcel, P. Lavalle, G. Decher, B. Senger, J.C. Voegel, P. Schaaf, Influence of the polyelectrolyte molecular weight on exponentially growing multilayer films in the linear regime, Langmuir 23 (2007) 1898–1904, http://dx.doi.org/10.1021/la062728k.
[29] P. Kujawa, P. Moraille, J. Sanchez, A. Badia, F.M. Winnik, Effect of molecular weight on the exponential growth and morphology of hyaluronan/chitosan multilayers: a surface plasmon resonance spectroscopy and atomic force microscopy investigation, J. Am. Chem. Soc. 127 (2005) 9224–9234, http://dx.doi.org/10.1021/ja044385n.
[30] M. Mihai, I. Stoica, S. Schwarz, PH-sensitive nanostructured architectures based on synthetic and/or natural weak polyelectrolytes, Colloid Polym. Sci. 289 (2011) 1387–1396, http://dx.doi.org/10.1007/s00396-011-2462-4.
[31] D. Mu, J.-Q. Li, S.-Y. Feng, Mesoscopic simulation of the self-assembly of the weak polyelectrolyte poly(ethylene oxide)-block-poly(methyl methacrylate) diblock copolymers, Soft Matter 11 (2015) 4366–4374, http://dx.doi.org/10.1039/C5SM00346F.
[32] M. Elzbieciak, S. Zapotoczny, P. Nowak, R. Krastev, M. Nowakowska, P. Warszyński, Influence of pH on the structure of multilayer films composed of strong and weak polyelectrolytes, Langmuir 25 (2009) 3255–3259, http://dx.doi.org/10.1021/la803988k.
[33] S.E. Burke, C.J. Barrett, PH-responsive properties of multilayered poly(L-lysine)/hyaluronic acid surfaces, Biomacromolecules 4 (2003) 1773–1783, http://dx.doi.org/10.1021/bm034184w.
[34] T. Mauser, C. Déjugnat, G.B. Sukhorukov, Balance of hydrophobic and electrostatic forces in the ph response of weak polyelectrolyte capsules, J. Phys. Chem. B. 110 (2006) 20246–20253, http://dx.doi.org/10.1021/jp063502t.
[35] S. Wang, S. Granick, J. Zhao, Charge on a weak polyelectrolyte, J. Chem. Phys. 129 (2008), http://dx.doi.org/10.1063/1.3055596.
[36] J. Song, T. Qiu, Y. Chen, W. Zhang, L.-J. Fan, Layer-by-layer introduction of poly (phenylenevinylene) onto microspheres and probing the influence from the weak/strong polyanion spacer-layers, J. Colloid Interface Sci. 452 (2015) 190–198, http://dx.doi.org/10.1016/j.jcis.2015.04.024.
[37] E. Costa, M.M. Lloyd, C. Chopko, A. Aguiar-Ricardo, P.T. Hammond, Tuning smart microgel swelling and responsive behavior through strong and weak polyelectrolyte pair assembly, Langmuir 28 (2012) 10082–10090, http://dx.doi.org/10.1021/la301586t.
[38] A. Foster, Development of Biocompatible Aptamer Films as Smart Materials for Novel Fertilizer Systems, Carleton University, 2013.
[39] C. Wilson, J.W. Szostak, Isolation of a fluorophore-specific redox activity DNA aptamer with weak redox activity, Chem. Biol. (1998), http://dx.doi.org/10.1016/S1074-5521(98)90289-7.
[40] B.G. De Geest, A.M. Jonas, J. Demeester, S.C. De Smedt, Glucose-responsive polyelectrolyte capsules, Langmuir 22 (2006) 5070–5074, http://dx.doi.org/10.1021/la053368o.
[41] H. Inoue, K. Sato, J.I. Anzai, Disintegration of layer-by-layer assemblies composed of 2-iminobiotin-labeled poly(ethyleneimine) and avidin, Biomacromolecules 6 (2005) 27–29, http://dx.doi.org/10.1021/bm0495856.
[42] D.T. Haynie, N. Palath, Y. Liu, B. Li, N. Pargaonkar, Biomimetic nanostructured materials: Inherent reversible stabilization of polypeptide microcapsules, Langmuir 21 (2005) 1136–1138, http://dx.doi.org/10.1021/la047833d.
[43] B.G. De Geest, A.G. Skirtach, A.A. Mamedov, A.A. Antipov, N.A. Kotov, S.C. De Smedt, et al., Ultrasound-triggered release from multilayered capsules, Small 3 (2007) 804–808, http://dx.doi.org/10.1002/smll.200600441.
[44] S. Erokhina, L. Benassi, P. Bianchini, A. Diaspro, V. Erokhin, M.P. Fontana, Light-driven release from polymeric microcapsules functionalized with bacteriorhodopsin, J. Am. Chem. Soc. 131 (2009) 9800–9804, http://dx.doi.org/10.1021/ja903066s.
[45] F. Wang, J. Feng, W. Tong, C. Gao, A facile pathway to fabricate microcapsules by in situ polyelectrolyte coacervation on poly(styrene sulfonate)-doped $CaCO_3$ particles, J. Mater. Chem. 17 (2007) 670, http://dx.doi.org/10.1039/b612534d.
[46] D.V. Volodkin, A.I. Petrov, M. Prevot, G.B. Sukhorukov, Matrix polyelectrolyte microcapsules: new system for macromolecule encapsulation, Langmuir 20 (2004) 3398–3406, http://dx.doi.org/10.1021/la036177z.
[47] K. Büscher, K. Graf, H. Ahrens, C.A. Helm, Influence of adsorption conditions on the structure of polyelectrolyte multilayers, Langmuir 18 (2002) 3585–3591, http://dx.doi.org/10.1021/la011682m.
[48] R.A. McAloney, M. Sinyor, V. Dudnik, M. Cynthia Goh, Atomic force microscopy studies of salt effects on polyelectrolyte multilayer film morphology, Langmuir 17 (2001) 6655–6663, http://dx.doi.org/10.1021/la010136q.